Supporting Information for Potential effect of the marine carbon cycle on the multiple equilibria window of the Atlantic Meridional Overturning Circulation"

A. Boot[1], A. S. Von der Heydt[1,2], and H. A. Dijkstra[1,2]

[1]Institute for Marine and Atmospheric research Utrecht, Department of Physics,Utrecht University, Utrecht, the Netherlands

[2]Center for Complex Systems Studies, Utrecht University, Utrecht, the Netherlands

Contents of this file

Introduction The supplementary information includes a more extensive description of both the ocean circulation and the carbon cycle box model, the way they are coupled and

how the model equations are solved. Supplementary tables are given with information about the considered cases, and the parameter values. Supplementary figures include the CMIP6 fits, additional cases, and the model sensitivity to E_s.

The ocean circulation box model

The box model representing the dynamics of the AMOC simulates the depth of the pycnocline and the distribution of salt in the Atlantic Ocean and the Southern Ocean. It consists of 5 boxes, and therefore 6 prognostic variables. The northern box n represents the regions of deep water formation in the North Atlantic and box s represents the entire Southern Ocean (i.e. all longitudes). There are two thermocline boxes t and ts where box ts represents the region between 30°S and 40°S which is characterized by strong sloping isopycnals where the pycnocline becomes shallower moving poleward. Underneath the four surface boxes, there is one box (d) representing the deep ocean.

The distribution of salinity in the model is dependent on the ocean circulation and freshwater fluxes. There are multiple volume fluxes in the model. In the Southern Ocean, there is wind-induced Ekman transport into the Atlantic (q_{Ek}), and there is an eddy induced transport from the Atlantic into the Southern Ocean (q_e) which is dependent on the pycnocline depth D. The difference between the two, defined as q_S, represents upwelling in the Southern Ocean and net volume transport into the Atlantic thermocline. The thermocline also is sourced with water from box d through diffusive upwelling (q_U). The strength of the downward branch of the AMOC is represented in the North Atlantic by q_N. This downwelling is dependent on the meridional density gradient between box ts and box n, where the density is determined using a linear equation of state. Wind driven

gyre transport is modelled by r_N in the Northern Hemisphere, and r_S in the Southern Hemisphere. Salinity is also affected by two surface freshwater fluxes, modelled as virtual salt fluxes. First, there is a symmetrical forcing E_s, i.e. the freshwater flux is the same for both hemispheres; and secondly, there is an asymmetrical forcing E_a which results in interhemispheric differences. This last parameter can be viewed as a hosing parameter for the AMOC strength since it regulates the salinity of box n. The pycnocline depth is an important state variable in this model since several volume fluxes are dependent on it. This depth is dependent on four different volume fluxes going in and out of the two thermocline boxes t and ts (q_e, q_{Ek}, q_U, q_N).

The model provides a simple framework to study AMOC dynamics and has already been used to show both slow (Cimatoribus et al., 2014) and fast, noise-induced (Castellana et al., 2019) tipping of the AMOC by freshwater forcing. However, several assumptions are made. The most important assumptions are that we neglect diapycnal mixing, and that temperature anomalies do not affect the AMOC strength (i.e. temperature is not a prognostic variable), since temperature anomalies have a faster decay timescales compared to salinity anomalies. Compared to earlier versions of the model we will use a different default value for E_s. In previous studies values of 0.25Sv (Cimatoribus et al., 2014) and 0.17Sv (Castellana et al., 2019) have been used. Here we choose a default value of 0.56Sv based on the CMIP6 multi model mean value at a CO_2 concentration of 300 ppm.

Satellite based observations of the HOAPS4.0 data (Andersson et al., 2017) show a net freshwater flux of 1 Sv averaged over the period 1987-2015 into the region representing the thermocline box. This results in an E_s value of 0.5Sv and therefore close to the chosen default value based on the CMIP6 ensemble. Basing the default value on the CMIP6 ensemble, instead of on observations, is done to enable use to easier compare the reference cases with cases where the CMIP6 fitted E_s (Eq. 1 and Eq. 2 in the main text) coupling is used. Since observational values are close to the CMIP6 multi model mean value, we consider the model to give an adequate representation of the Atlantic Ocean.

The carbon cycle box model

The carbon cycle model is based on the equations of the SCP-M (O'Neill et al., 2019). The original SCP-M has two terrestrial carbon stocks, an atmosphere box, and 7 ocean boxes representing the global ocean. In the ocean multiple tracers are simulated that are important for the marine carbon cycle. In this study, we do not use the terrestrial biosphere and we have adapted the box structure to represent the box structure of the ocean circulation model, which only represents the Atlantic Ocean and the Southern Ocean. Some assumptions had to be made here. First of all, the depth of boxes n and s is not given in Cimatoribus et al. (2014) but is necessary for the carbon cycle model. We assume these to be 300 m. The total depth of the ocean is assumed to be 4000 m. Secondly, the riverine fluxes in the SCP-M represent the entire global riverine input, while the circulation model only simulates a part of the global domain. We use a volume fraction (volume circulation model / volume SCP-M = 0.2) to scale the river fluxes.

Another adaption we have made is that we only use three tracers: dissolved inorganic carbon (DIC), alkalinity (Alk), and phosphate (PO_4). All tracers are affected by the dynamical circulation simulated in the ocean circulation model in a similar fashion as salinity. DIC is affected by biological production and remineralization (soft tissue pump), the formation and dissolution of calcium carbonate ($CaCO_3$; carbonate pump), and gas exchange with the atmosphere. Alk is only affected by the carbonate pump, and PO_4 only by the soft tissue pump. All three tracers have a riverine source flowing into box t and a sink to the sediments. PO_4 is explicitly conserved in the system, i.e. the source of PO4 is equal to the sink of PO4 at all times. DIC and Alk, however, can vary since the time dependent riverine influx is not necessarily equal to the sediment outflux. The change in total carbon (DIC + atmospheric CO_2) and Alk in the atmosphere-ocean system can be captured in two ODEs as the sum of riverine influx and the sediment outflux. The riverine influx is a function of atmospheric pCO_2 and represents the weathering of silicate and carbonate rocks i.e.,

$$C_{river} = W_{carb,c} + (W_{carb,v} + W_{si}) \times CO_2^{atm} \tag{1}$$

The sediment outflux of DIC is determined by the sum of the soft tissue and the carbonate pumps over the entire ocean. In this model, generally all produced organic matter is also remineralized, causing the contribution of the soft tissue pump to be negligible resulting in

$$C_{sed} = C_{river} \times V_t + \sum_{i=1}^{5} (C_{carb,i} \times V_i) \tag{2}$$

Without the influence of the soft tissue pump, the change in total carbon and total Alk are proportional, where the change in total Alk is twice as big as the change in total carbon. For the dissolution of $CaCO_3$ and the gas exchange of carbon, the pH needs to be determined. In the original SCP-M a simple function is used where the pH of timestep i-1 is used as an initial guess for timestep i (Follows et al., 2006). As long as the changes per time step remain relatively small, this scheme is sufficiently accurate. However, due to our solution method, in which steady states are calculated versus parameters, this function is not suitable for this study. Therefore, we have chosen a simple 'text-book' carbonate chemistry (Williams & Follows, 2011; Munhoven, 2013) where Alk is assumed to be equal to carbonate alkalinity ($Alk_{carb} = [HCO_3^-]+[CO_3^{2-}]$). This method is less accurate and leads to higher pH values (Munhoven, 2013) and lower atmospheric pCO_2 values (Boot et al., 2022). Since we use a different carbonate chemistry, the atmospheric pCO_2 values are relatively low. Furthermore, the model used in Boot et al. (2022) is tuned globally whereas here we only take the Atlantic and Southern Ocean into account. We therefore retune the model in order to approach CO_2 concentrations of around 300 ppm for cases REF and BIO. To accomplish this, we have retuned the export production (general decrease) and rain ratio (increase from 0.07 to 0.15). We have also chosen different values for the biological efficiencies in Eq. 4 below compared to Boot et al. (2022) to get similar atmospheric pCO_2 values for cases REF and BIO at $E_a = 0$ Sv.

Couplings and feedbacks in the model

The first coupling between the physical and the carbon cycle model is through the ocean circulation. The AMOC determined in the circulation model is used for the advec-

tive transport of the three tracers in the carbon cycle model providing a first coupling between the two models. We have implemented additional couplings between the model and specific feedbacks within the carbon cycle model. Several of these feedbacks have previously been introduced into the SCP-M (Boot et al., 2022).

As explained earlier, we have introduced a coupling between E_s and atmospheric pCO_2 (Eq. 1 and 2 in the main text; Fig. S1b). These are simple linear and logarithmic functions based on a fit to a CMIP6 multi-model mean forced under the 1% CO_2 increase scenario (Eyring et al., 2016). We have used 28 different models to determine the multi-model mean (Fig. S1a). A list of the used models and the references for the data can be found in a separate data sheet. We have used all models available, except for a few for which we had difficulty downloading the model data. Each model was first regridded to a rectilinear grid, then we integrated the freshwater flux over the region that represents the thermocline box of the box model and E_s was determined dividing this number by 2. After this, all models and the multi-model mean were smoothed with a 5-year moving mean. The regions used in the CMIP6 model are for box t the Atlantic Ocean between 50°N and 30°S. The fits represent a feedback that the subtropical ocean becomes drier while the subpolar regions in both the northern and the southern hemisphere become wetter under CO_2 forcing. This coupling is the only way how the carbon cycle model can influence the circulation model. Both fits are used in Section 3.1 of the main text since the fits have different behavior for pCO_2 values below 300 ppm. Also a different logarithmic coupling is used (Eq. 3 in the main text; Fig. S1c) to test the sensitivity to

different E_s-pCO_2 coupling strengths. This fit, is used in Section 3.1 and together with Eq. 2 also in Section 3.2.

The other two couplings are a one way coupling from the circulation model to the carbon cycle model. First, we introduce dilution fluxes to both DIC and Alk coupled to the freshwater fluxes E_s and E_a (Eq. 3). Increasing the concentrations of DIC and Alk due to evaporation and decreasing the concentrations due to a net influx of freshwater at the surface. Lastly, we create a dependency of the biological export production in the surface boxes to the amount of PO_4 advected into the specific surface box and therefore introducing a dependency on the ocean circulation (see below).

$$C_{dil,i} = \lambda_D \times (E_s + E_a) \times \frac{C_i}{V_i} \tag{3}$$

Where C_i is the tracer concentration in box i and V_i the volume, and λ_D is a parameter that determines whether the coupling is used ($\lambda_D = 1$) or not ($\lambda_D = 0$).

$$Z_i = (1 - \lambda_{BI}) \times Z_{i,base} + \lambda_{BI} \times (q_{j \to i} \times [PO_4^{3-}]_j + P_{river,t}) \times \epsilon_i \tag{4}$$

Here Z represents the export production, λ_{BI} a parameter to switch between the default value of Z ($Z_{i,base}$; $\lambda_{BI} = 0$) and the variable export production ($\lambda_{BI} = 1$). In addition, q represents the volume transport, P_{river} the riverine influx of PO_4 in box t, and ϵ_i represents a biological efficiency term.

Besides coupling the models, we also introduce (non-linear) feedbacks in the carbon cycle model. First of all, we allow the sea surface temperatures (SSTs) to vary with

atmospheric pCO_2 following a logarithmic function and a climate sensitivity parameter (Eq. 5 and 6):

$$T_i = T_{i,base} + \Delta T_i \tag{5}$$

$$\Delta T_i = \lambda_T \times 0.54\ times 5.35 \ln(\frac{CO_2}{CO_{2,0}}) \tag{6}$$

By varying the parameter λ_T we are able to change the climate sensitivity of the model. Changing the SSTs will also change the density in the ocean circulation model. However, since we use a linear equation of state and the change of SST is homogeneous over all boxes, it does not influence the dynamical ocean circulation and is therefore not a coupling but a feedback within the carbon cycle.

A second feedback we introduce is a linear temperature dependency in the biological efficiency which was introduced in the biological coupling (Eq. 7). Under an SST increase, the efficiency will decrease following

$$\epsilon_i = (\lambda_\epsilon \times -0.1\Delta T) + \epsilon_{i,base} \tag{7}$$

For this feedback it is necessary to also use the temperature feedback and the strength can be regulated with $\lambda_{epsilon}$.

The third feedback allows the piston velocity (k_w) to vary with the SSTs (Eq. 8). When the SST feedback is used, this also affects the piston velocity. The temperature dependency is introduced by making the piston velocity a function of the Schmidt number

(Eq. 9) following

$$k_{w,i} = (1 - \lambda_P) \times k_{w,ibase} + \lambda_P k_{w,ibase} \times (\frac{Sc_i}{660})^{-0.5} \tag{8}$$

Where

$$Sc_i = 2116.8 - 136.25T_i + 4.7353T_i^2 - 0.092307T_i^3 + 0.0007555T_i^4 \tag{9}$$

In this case the feedback can either be switched on ($\lambda_P = 1$) or off ($\lambda_P = 0$). Without this feedback the piston velocity is similar for all boxes, but with this feedback the piston velocity will differ per box. Lastly, we have introduced a feedback on the rain ratio (Eq. 10) making it dependent on the saturation state of $CaCO_3$ following

$$F_{Ca,i} = (1 - \lambda_F) \times F_{Ca,base} + \lambda_F \times 0.022(\frac{[Ca_i^{2+}][CO_3^{2-}]}{K_{sp,i}})^{0.81} \tag{10}$$

Similar as for the piston velocity λ_F is either 0 or 1, and including this feedback will introduce different rain ratios per box. In the main text only cases using the biological coupling (BIO), the E_s-coupling (E_s) and the rain ratio (FCA) have been shown. In the supplementary material more simulations, also using the couplings and feedbacks described above, are shown.

Model equations There are in total 21 state variables: salinity, DIC, alkalinity, and PO_4 in the 5 boxes, and the pycnocline depth D. The state variables in the deep box are determined using conservation laws. The salinity equations are given by Eq. 12-15, the pycnocline depth is determined using Eq. 16.

$$\frac{d(V_t S_t)}{dt} = q_S(\theta(q_S)S_{ts} + \theta(-q_S)S_t + q_U S_d - \theta(q_N)q_N S_t + r_s(S_{ts} - S_t) + r_N(S_n - S_t) + 2E_s S_0 \tag{11}$$

$$\frac{d(V_{ts}S_{ts})}{dt} = q_{Ek}S_s - q_eS_{ts} - q_S(\theta(q_S)S_{ts} + \theta(-q_S)S_t) + r_S(S_t - S_{ts}) \tag{12}$$

$$V_n\frac{dS_n}{dt} = \theta(q_N)q_N(S_t - S_n) + r_N(S_t - S_n) - (E_s + E_a)S_0 \tag{13}$$

$$V_s\frac{dS_s}{dt} = q_S(\theta(q_S)S_d + \theta(-q_S)S_s) + q_eS_{ts} - q_{Ek}S_s - (E_s - E_a)S_0 \tag{14}$$

$$(A + \frac{L_{xA}L_y}{2})\frac{dD}{dt} = q_U + q_{Ek} - q_e - \theta(q_N)q_N \tag{15}$$

$$S_0V_0 = V_nS_n + V_dS_d + V_tS_t + V_{ts}S_{ts} + V_sS_s \tag{16}$$

Where:

$$q_{Ek} = \frac{\tau L_{xS}}{\rho_0|f_S|} \tag{17}$$

$$q_e = A_{GM}\frac{L_{xA}}{L_y}D \tag{18}$$

$$q_U = \frac{\kappa A}{D} \tag{19}$$

$$q_N = \eta\frac{\rho_n - \rho_{ts}}{\rho_0}D^2 \tag{20}$$

$$q_S = q_{Ek} - q_e \tag{21}$$

$$\rho_i = \rho_0(1 - \alpha(T_i - T_0) + \beta(S_i - S_0)) \tag{22}$$

$$\frac{d[DIC]_i}{dt} = C_{phys,i} + C_{bio,i} + C_{carb,i} + C_{air,i} + C_{river,t} \tag{23}$$

$$\frac{d[Alk]_i}{dt} = A_{phys,i} + A_{carb,i} + A_{river,t} \tag{24}$$

$$\frac{d[PO_4^{3-}]_i}{dt} = P_{phys,i} + P_{bio,i} + P_{river,t} \tag{25}$$

$$\frac{dC_{tot}}{dt} = C_{river,t} \times V_t + \sum_{i=1}^{5}(C_{carb,i}V_i) + \sum_{i=1}^{5}(C_{bio,i}V_i) \tag{26}$$

In these equations the different terms represent advective fluxes (X_{phys}), biological fluxes (X_{bio}), carbonate fluxes (X_{carb}), air-sea gas exchange (C_{air}) and the river influx (X_{river}), which are determined following:

$$X_{phys,i} = \frac{1}{V_i}(\sum_{i=1}(q_{j\to i} \times X_j) - \sum_{i=1}(q_{i\to j} \times X_i)) \tag{27}$$

This equation represents that the concentration X changes through an advective flux flowing out of box i to box j ($q_{i\to j}$ times the concentration in box i (X_i), and a flux flowing

into box i from box j ($q_{j\to i}$) times the concentration in box j (X_j). There can be fluxes from multiple boxes into one box.

$$C_{air.i} = \frac{K_{0,i} \times k_{w,i} \times \rho_0 \times (CO_2^{atm} - pCO_{2,i})}{V_i} \tag{28}$$

For i is n, t, ts or s. K_0 is the solubility constant, k_w the piston velocity, CO_2^{atm} the atmospheric CO_2 concentration, pCO_2 the partial pressure of CO_2 in the ocean and V the volume of the ocean box.

$$C_{carb.i} = -\frac{Z_i t \times A_{iCa,i}}{V_i} + ([CO_3^{2-}]_i[Ca^{2+}]_i)\rho_0 k_{Ca}(1 - \frac{([CO_3^{2-}]_i[Ca^{2+}]_i)}{K_{sp,i}})^n \times PerC + DC \tag{29}$$

For i is n, t, ts, or s. Z represent biological production, A the surface area of the box, F_{Ca} the rain ratio and V the volume. Other variables are the carbonate ion concentration ($[CO_3^{2-}]$), calcium concentration ($[Ca^{2+}]$), and equilibrium constant for $CaCO_3$ dissolution (K_{sp}).

$$C_{bio,i} = \frac{Z_i \times A_i}{V_i} \times (\frac{d_{fi}}{d_0})^{-b} \tag{30}$$

For i is n, t, ts or s. Z represent biological production, A the surface area of the box, V the volume, and d_{fi} the floor depth of the box.

$$A_{carb.i} = 2 \times C_{carb.i} \tag{31}$$

$$P_{bio,i} = r_{P:C} \times C_{bio,i} \tag{32}$$

An explanation and the value of all parameters are given in the tables in this document.

The solution method

Our coupled system is a system of 22 ODEs (four tracers per box, the pycnocline depth and atmospheric pCO_2) of the form

$$\frac{d\mathbf{u}}{dt} = f(\mathbf{u}(t), \mathbf{p}) \tag{33}$$

Here $\mathbf{u}$ is the state vector (containing all the dependent quantities in all boxes), f contains the right-hand-side of the equations and $\mathbf{p}$ is the parameter vector. To solve this system of equations we use the continuation software AUTO-07p (Doedel et al., 2007). Both the circulation model (Cimatoribus et al., 2014), and the SCP-M (Boot et al., 2022) have already been implemented in the software before. AUTO enables us to efficiently compute branches of stable and unstable steady state solutions under a varying control parameter. Furthermore, it allows for detection of special points such as saddle-node bifurcations, which is important for determining the multiple equilibria window of the AMOC. However, one of the requirements of AUTO is that the Jacobian of the system is non-singular. To achieve this, we use explicit conservation equations (Eq. 16 and 26) to eliminate the ODEs of the deep box. Both the conservation equation of salt (Eq. 16) and PO_4 are already explicitly included into the model. However, as described previously, this is not the case for DIC and Alk. Therefore, we have to introduce an extra ODE describing the change in total carbon in the system (Eq. 26). Since the change in alkalinity in the

system is proportional to the change in total carbon, only one extra ODE is necessary. By eliminating the ODEs for the deep box and introducing the ODE for total carbon in the ocean-atmosphere system, AUTO can solve the system with 19 ODEs. AUTO has three accuracy parameters. The absolute and relative accuracy differ per specific case, but are set to maximal 5×10^{-3}. The accuracy for the detection of special points (e.g. saddle nodes and Hopf bifurcations) is set to 10^{-5}.

References

Andersson, A., Graw, K., Schröder, M., Fennig, K., Liman, J., Bakan, S., ... Klepp, C. (2017). *Hamburg Ocean Atmosphere Parameters and Fluxes from Satellite Data - HOAPS 4.0.* Satellite Application Facility on Climate Monitoring (CM SAF). Retrieved from `https://wui.cmsaf.eu/safira/action/viewDoiDetails?acronym=HOAPS{\_}V002` doi: 10.5676/EUM_SAF_CM/HOAPS/V002

Boot, A., von der Heydt, A. S., & Dijkstra, H. A. (2022). Effect of the Atlantic Meridional Overturning Circulation on atmospheric pCO$_{2}$ variations. *Earth System Dynamics*, *13*(3), 1041–1058. Retrieved from `https://esd.copernicus.org/articles/13/1041/2022/` doi: 10.5194/esd-13-1041-2022

Castellana, D., Baars, S., Wubs, F. W., & Dijkstra, H. A. (2019). Transition Probabilities of Noise-induced Transitions of the Atlantic Ocean Circulation. *Scientific Reports*, *9*(1), 20284. Retrieved from `https://doi.org/10.1038/s41598-019-56435-6` doi: 10.1038/s41598-019-56435-6

Cimatoribus, A. A., Drijfhout, S. S., & Dijkstra, H. A. (2014). Meridional overturning circulation: stability and ocean feedbacks in a box model. *Climate Dynamics*, *42*(1),

311–328. Retrieved from https://doi.org/10.1007/s00382-012-1576-9 doi: 10.1007/s00382-012-1576-9

Doedel, E. J., Paffenroth, R. C., Champneys, A. C., Fairgrieve, T. F., Kuznetsov, Y. A., Oldeman, B. E., ... Wang, X. J. (2007). *AUTO-07p: Continuation and Bifurcation Software for Ordinary Differential Equations.*

Eyring, V., Bony, S., Meehl, G. A., Senior, C. A., Stevens, B., Stouffer, R. J., & Taylor, K. E. (2016, may). Overview of the Coupled Model Intercomparison Project Phase 6 (CMIP6) experimental design and organization. *Geosci. Model Dev.*, *9*(5), 1937–1958. Retrieved from https://gmd.copernicus.org/articles/9/1937/2016/https://gmd.copernicus.org/articles/9/1937/2016/gmd-9-1937-2016.pdf doi: 10.5194/gmd-9-1937-2016

Follows, M. J., Ito, T., & Dutkiewicz, S. (2006). On the solution of the carbonate chemistry system in ocean biogeochemistry models. *Ocean Modelling*, *12*(3), 290–301. Retrieved from http://www.sciencedirect.com/science/article/pii/S1463500305000533 doi: https://doi.org/10.1016/j.ocemod.2005.05.004

Lueker, T. J., Dickson, A. G., & Keeling, C. D. (2000). Ocean pCO2 calculated from dissolved inorganic carbon, alkalinity, and equations for K1 and K2: validation based on laboratory measurements of CO2 in gas and seawater at equilibrium. *Marine Chemistry*, *70*(1), 105–119. Retrieved from https://www.sciencedirect.com/science/article/pii/S0304420300000220 doi: https://doi.org/10.1016/S0304-4203(00)00022-0

Millero, F. J. (1983). CHAPTER 43 - Influence of Pressure on Chemical Processes in the Sea. In J. P. RILEY & R. B. T. C. O. CHESTER (Eds.), (pp. 1–88). Academic Press. Retrieved from https://www.sciencedirect.com/science/article/pii/B9780125886086500079 doi: https://doi.org/10.1016/B978-0-12-588608-6.50007-9

Mucci, A. (1983, sep). The solubility of calcite and aragonite in seawater at various salinities, temperatures, and one atmosphere total pressure. *American Journal of Science*, *283*, 780–799. Retrieved from https://ui.adsabs.harvard.edu/abs/1983AmJS..283..780M doi: 10.2475/ajs.283.7.780

Munhoven, G. (2013). Mathematics of the total alkalinity–pH equation - pathway to robust and universal solution algorithms: the SolveSAPHE package v1.0.1. *Geoscientific Model Development*, *6*(4), 1367–1388. Retrieved from https://gmd.copernicus.org/articles/6/1367/2013/ doi: 10.5194/gmd-6-1367-2013

O'Neill, C. M., Hogg, A. M., Ellwood, M. J., Eggins, S. M., & Opdyke, B. N. (2019). The [simple carbon project] model v1.0. *Geoscientific Model Development*, *12*(4), 1541–1572. Retrieved from https://gmd.copernicus.org/articles/12/1541/2019/ doi: 10.5194/gmd-12-1541-2019

Weiss, R. F. (1974). Carbon dioxide in water and seawater: the solubility of a non-ideal gas. *Marine Chemistry*, *2*(3), 203–215. Retrieved from https://www.sciencedirect.com/science/article/pii/0304420374900152 doi: https://doi.org/10.1016/0304-4203(74)90015-2

Williams, R. G., & Follows, M. J. (2011). *Ocean Dynamics and the Carbon Cycle: Principles and Mechanisms*. Cambridge: Cambridge University Press.

Table S1. Overview of the used cased in the main text. The left column represents the used simulations, where the uncoupled case is added to show the coupling of the carbon cycle in REF. The other columns represent whether a coupling or feedback denoted in the top row is used in the case mentioned in the first column.

Case name	Carbon cycle	BIO	E_s	FCA
Uncoupled				
REF	X			
BIO	X	X		
E_s + BIO	X	X	X	
E_s + BIO + FCA	X	X	X	X

Table S2. Additional cases not included in the main text using additional feedbacks as described in this document. When the E_s-coupling is used, the logarithmic CMIP6 fit (Eq. 2 in the main text

is used. Results of these cases can be seen in Figure S2.

Notation	S-1	S-2	S-3	S-4	S-5	S-6	S-7	S-8	S-9	S-10
λ_{BI}	1	1	1	1	1	1	1	1	1	1
λ_T	1	0	0	1	1	1	0	0	1	1
λ_P	0	0	1	1	1	0	0	1	1	1
λ_D	0	1	0	0	0	0	1	0	0	0
λ_ϵ	0	0	0	0	1	0	0	0	0	1
E_s	0	0	0	0	0	Eq. 2	Eq. 2	Eq. 2	Eq. 2	Eq. 2

Table S3. Symbol (column 1), description (column 2), value (column 3), and units (column 4) of the general parameters used in the ocean circulation model based on Cimatoribus et al. (2014).

Symbol	Description	Value	Units
V_0	Total volume of the basin	3×10^{17}	m^3
V_n	Volume of box n	3×10^{15}	m^3
V_s	Volume of box s	9×10^{15}	m^3
A_t	Surface area box t	1×10^{14}	m^2
L_{xA}	Zonal extent of the Atlantic Ocean at its southern end	1×10^7	m
L_y	Meridional extent of the frontal region of the Southern Ocean	1×10^6	m
L_{xS}	Zonal extent of the Southern Ocean	3×10^7	m
τ	Average zonal wind stress amplitude	0.1	N m^{-2}
A_{GM}	Eddy diffusivity	1700	m^2 s^{-1}
f_S	Coriolis parameter	-1×10^{-4}	s^{-1}
ρ_0	Reference density	1027.5	kg m^{-3}
κ	Vertical diffusivity	1×10^{-5}	m^2 s^{-1}
S_0	Reference salinity	35	g/kg
T_0	Reference temperature	5	°C
$T_{n,base}$	Base temperature box n	5	°C
$T_{ts,base}$	Base temperature box ts	10	°C
η	Hydraulic constant	3×10^4	m s^{-1}
α	Thermal expansion coefficient	2×10^{-4}	K^{-1}
β	Haline contraction coefficient	8×10^{-4}	$(g/kg)^{-1}$
r_S	Transport by the southern subtropical gyre	10×10^6	m^3 s^{-1}
r_N	Transport by the northern subtropical gyre	5×10^6	m^3 s^{-1}
E_s	Symmetric freshwater flux	0.56×10^6	m^3 s^{-1}

Table S4. Symbol (column 1), description (column 2), value (column 3), and units (column 4) of the general parameters used in the ocean circulation model added or changed with respect to Cimatoribus et al. (2014)

Symbol	Description	Value	Units
E_s	Symmetric freshwater flux	0.56×10^6	m^3 s^{-1}
d_{fn}	Floor depth Box n	300	m
d_{ft}	Floor depth Box t	variable (D)	m
d_{fts}	Floor depth Box ts	variable (D)	m
d_{fs}	Floor depth Box s	300	m
d_{fd}	Floor depth Box d	4000	m
$T_{t,base}$	Base temperature Box t	23.44	°C
$T_{s,base}$	Base temperature Box s	0.93	°C
T_d	Temperature Box d	1.8	°C

Table S5. Symbol (column 1), description (column 2), value (column 3), and units (column 4) of the general parameters used in the carbon cycle model based on Boot et al. (2022).

Symbol	Description	Value	Units
V_{at}	Volume of the atmosphere	1.76×10^{20}	m^3
$F_{Ca,base}$	Base rain ratio	0.07	-
n	Order of $CaCO_3$ dissolution kinetics	1	-
P_C	Mass percentage of C in $CaCO_3$	0.12	-
D_{Ca}	Constant dissolution rate of $CaCO_3$	2.75×10^{-13}	mol m^{-3} s^{-1}
W_{SC}	Constant silicate weathering	2.4×10^{-12}	mol m^{-3} s^{-1}
W_{SV}	Variable silicate weathering parameter	1.6×10^{-8}	mol m^{-3} atm^{-1} s^{-1}
W_{CV}	Variable carbonate weathering parameter	6.3×10^{-8}	mol m^{-3} atm^{-1} s^{-1}
k_{Ca}	Constant $CaCO_3$ dissolution rate	4.4×10^{-6}	s^{-1}
b	Exponent in Martin's law	0.75	-
d_0	Reference depth for biological productivity	100	m
$k_{w,base}$	Base piston velocity	3	m/day
$R_{C:P}$	Redfield C:P ratio	130	mol C/mol P
$R_{P:C}$	Redfield P:C ratio	1/130	mol P/mol C
$[Ca]_n$	Calcium concentration Box n	$0.01028 \times S_n$	mol m^{-3}
$[Ca]_t$	Calcium concentration Box t	$0.01028 \times S_t$	mol m^{-3}
$[Ca]_{ts}$	Calcium concentration Box ts	$0.01028 \times S_{ts}$	mol m^{-3}
$[Ca]_s$	Calcium concentration Box s	$0.01028 \times S_s$	mol m^{-3}
$[Ca]_d$	Calcium concentration Box d	$0.01028 \times S_d$	mol m^{-3}

Table S6. Symbol (column 1), description (column 2), value (column 3), and units (column 4) of the parameters used in the carbon cycle model that have been changed compared to Boot et al. (2022).

Symbol	Description	Value	Units
$Z_{n,base}$	Base biological production Box n	1.9	mol C m^{-2} yr^{-1}
$Z_{t,base}$	Base biological production Box t	2.1	mol C m^{-2} yr^{-1}
$Z_{ts,base}$	Base biological production Box ts	2.1	mol C m^{-2} yr^{-1}
$Z_{s,base}$	Base biological production Box s	1.1	mol C m^{-2} yr^{-1}
$\epsilon_{n,base}$	Base biological efficiency Box n	0.1	-
$\epsilon_{t,base}$	Base biological efficiency Box t	0.5	-
$\epsilon_{ts,base}$	Base biological efficiency Box ts	0.3	-
$\epsilon_{s,base}$	Base biological efficiency Box s	0.1	-
R_{PO4}	River influx of PO_4^{3-}	0.3×10^4	

Table S7. The symbols and description of the equilibrium constants are presented in the first two columns. The third column presents the source of the used expression.

Symbol	Description	Expression
K_0	Solubility constant	Weiss (1974)
K_1	First dissociation constant of carbonic acid	Lueker, Dickson, and Keeling (2000)
K_2	Second dissociation constant of carbonic acid	Lueker et al. (2000)
$K_{sp,base}$	Equilibrium constant for $CaCO_3$ dissolution	Mucci (1983)
$K_{sp,press}$	Pressure correction for $K_{sp,base}$	Millero (1983)

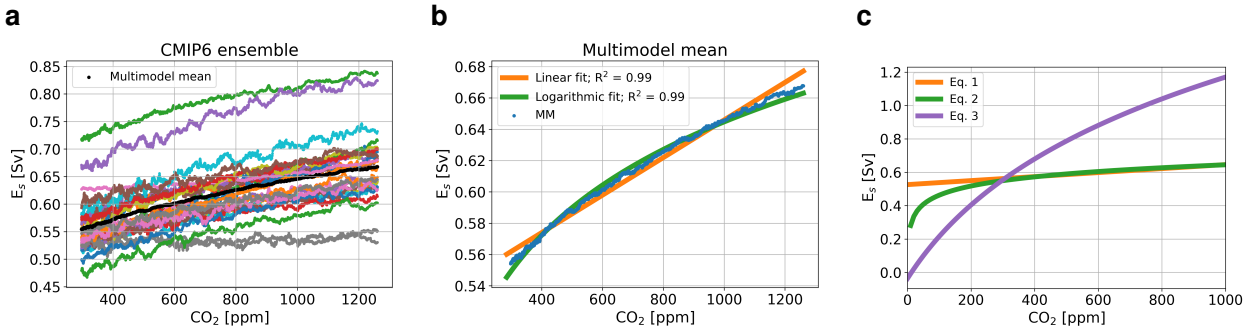

Figure S1. Symmetrical surface freshwater flux in Sv fitted to atmospheric pCO_2 in a CMIP6 ensemble of 28 models. In panel a the colored lines represent CMIP6 models and the black line represents the multi-model mean. In panel b the multi-model mean (blue) and linear (orange) and logarithmic (green) fits are shown including the R^2 values in the legend. In panel c the used fits used in the main text are displayed. The orange and green lines are similar to the ones in panel b. Orange represents Eq. 1, green Eq. 2, purple Eq. 3 (equations from main text).

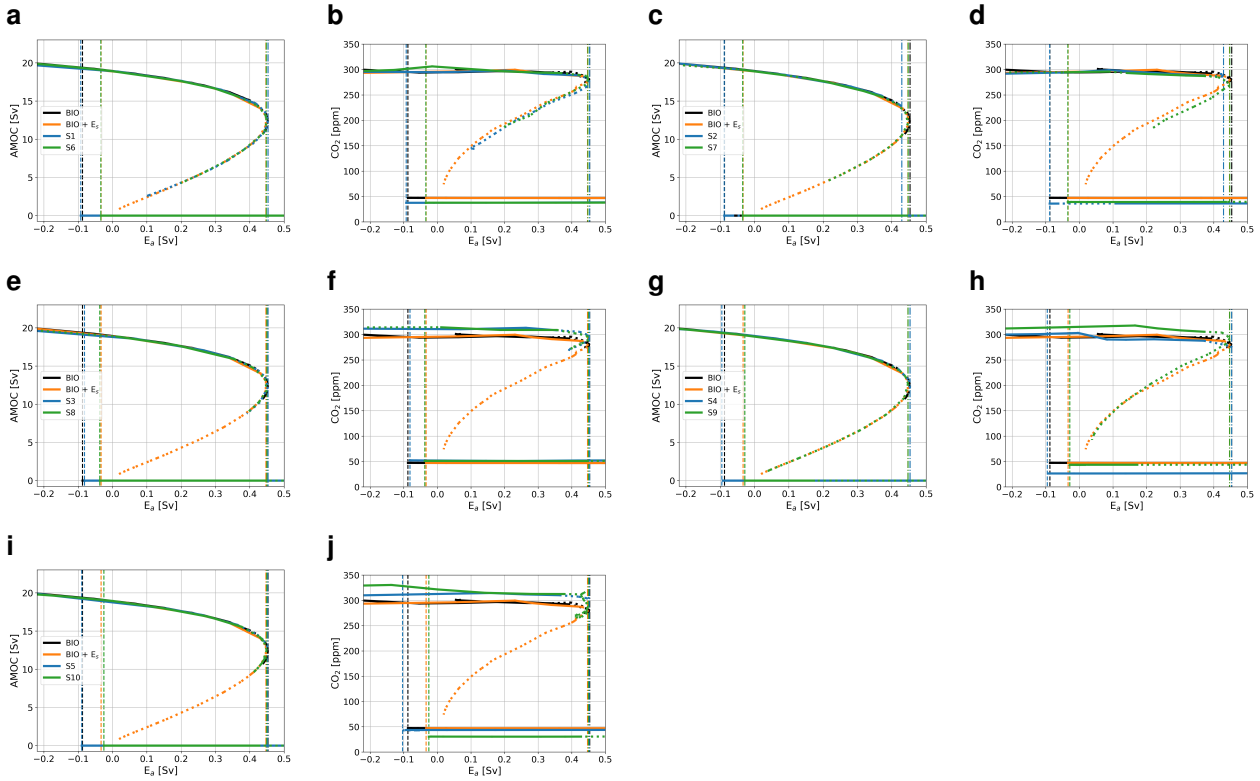

Figure S2. Bifurcation diagrams showing the sensitivity of the model to E_a for additional cases as defined in Table S2. Solid lines represent stable steady state solutions, dotted lines represent unstable states, dash-dotted lines represent the location of the saddle node on the on-branch, and dashed lines the location of the saddle node on the off-branch. The black lines represent a case with only the biological coupling (BIO), the orange lines with the logarithmic CMIP6 based E_s and biological coupling (E_s + BIO), and the blue and green lines represent the cases defined in Table S2. Results are for the AMOC strength in Sv (a, c, e, g, i) and atmospheric pCO_2 in ppm (b, d, f, h, j).

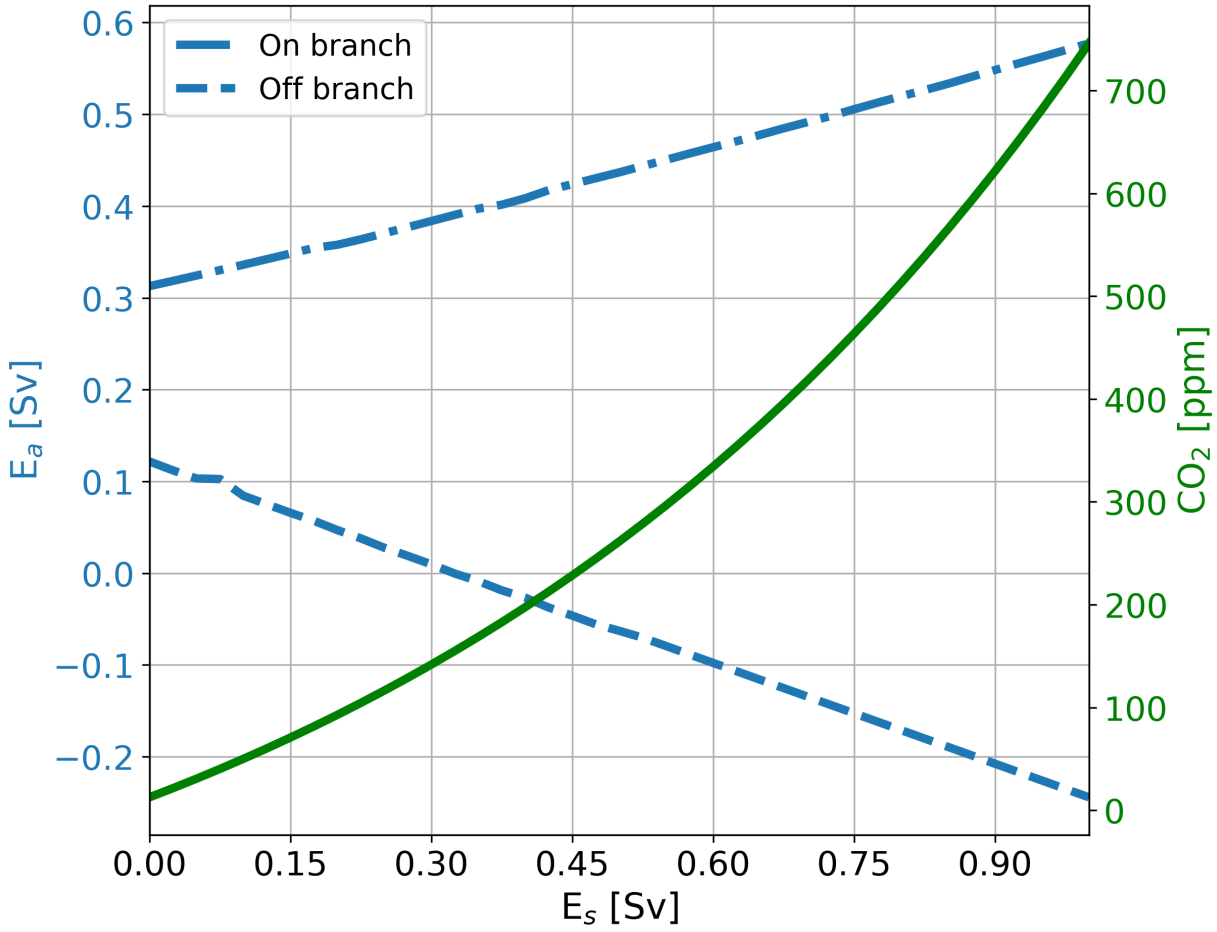

Figure S3. Sensitivity of the location in E_a of the saddle nodes in the circulation model to different values of E_s. The blue dashed dotted line represents the saddle node on the on-branch, and the blue dashed line the saddle node on the off branch. The green line, corresponding to the right y-axis, represents CO_2 concentrations in ppm corresponding to the strong E_s-pCO_2-coupling from the main text (Eq. 3) for the E_s values on the x-axis.